

Article

Removal of Organoselenium from Aqueous Solution by Nanoscale Zerovalent Iron Supported on Granular Activated Carbon

Stanley Onyinye Okonji ¹, Gopal Achari ^{2,*} and David Pernitsky ³

¹ Department of Mechanical and Manufacturing Engineering, University of Calgary, Calgary, AB T2N 1N4, Canada; stanley.okonji@ucalgary.ca

² Department of Civil and Environmental Engineering, University of Calgary, Calgary, AB T2N 1N4, Canada

³ Stantec Inc., Calgary, AB T2A 7H8, Canada; david.pernitsky@stantec.com

* Correspondence: gachari@ucalgary.ca

Abstract: Nanoscale zerovalent iron particles (nZVI) immobilized on coconut shell-based granular activated carbon (GAC) were studied to remove organoselenium from wastewater. A chemical reduction technique that involves the application of sodium borohydride was adopted for the adsorbent preparation. The texture, morphology and chemical composition of the synthesized adsorbents were analyzed with a scanning electron microscope (SEM), nitrogen adsorption–desorption isotherms and X-ray diffraction (XRD). Batch experiment with various pHs and contact times were conducted to evaluate nZVI/GAC adsorption performance. The results showed that nZVI/GAC has a strong affinity to adsorb selenomethionine (SeMet) and selenocysteine (SeCys) from wastewaters. The maximum removal efficiency for the composite (nZVI/GAC) was 99.9% for SeCys and 78.2% for SeMet removal, which was significantly higher than that of nZVI (SeCy, 59.2%; SeMet, 10.8%). The adsorption kinetics were studied by pseudo-first-order (PFO) and pseudo-second-order (PSO) kinetic models. Amongst the two, PSO seemed to have a better fit (SeCy, $R^2 > 0.998$; SeMet, $R^2 > 0.999$). The adsorption process was investigated using Langmuir and Freundlich isotherm models. Electrostatic attraction played a significant role in the removal of organoselenium by nZVI/GAC adsorption. Overall, the results indicated that GAC-supported nZVI can be considered a promising and efficient technology for removing organoselenium from wastewater.

Keywords: selenium; organoselenium; selenomethionine; selenocysteine; nanocomposite–nZVI/GAC; adsorption kinetics; wastewater treatment; isotherm studies



Citation: Okonji, S.O.; Achari, G.; Pernitsky, D. Removal of Organoselenium from Aqueous Solution by Nanoscale Zerovalent Iron Supported on Granular Activated Carbon. *Water* **2022**, *14*, 987. <https://doi.org/10.3390/w14060987>

Academic Editors: Carmen Teodosiu and Ruben Miranda

Received: 7 February 2022

Accepted: 17 March 2022

Published: 21 March 2022

Publisher's Note: MDPI stays neutral with regard to jurisdictional claims in published maps and institutional affiliations.



Copyright: © 2022 by the authors. Licensee MDPI, Basel, Switzerland. This article is an open access article distributed under the terms and conditions of the Creative Commons Attribution (CC BY) license (<https://creativecommons.org/licenses/by/4.0/>).

1. Introduction

Selenium is an interesting element, it is highly toxic for biotic and physiological well-being at high concentrations but is necessary at trace levels. Chronic exposure to elevated concentrations of selenium can result in central nervous disease, dermatitis, nephrosis, skeletal dysfunction, hepatic cancer and genotoxicity, among others [1–3]. Selenium can be classified into inorganic and organic selenium.

Primarily, the main species by which organic selenium are absorbed by plants and aquatic organisms in the environment are SeMet and SeCys [4,5]. These exist in wastewaters, especially those of coal fire power plants, mining sites, and oil and gas refineries [6]. These species of selenium have higher bioavailability as they are readily absorbed in animal and human digestive tracks; hence, they have a higher threshold of toxicity [5,7,8]. Another concern of organoselenium is the propensity to accumulate in living organisms for a long time, which can cause contamination of wildlife diet [9]. As a result, SeMet and SeCys are contaminants of concern in the environment; however, there are limited studies on removal methods [10]. Therefore, an effective treatment technology is required for the remediation of organic selenium from wastewater.

Currently, only a few studies have investigated the removal of organic selenium from wastewaters and industrial effluents. In general, the removal techniques reported include physico-chemical precipitation [11], chemical reduction [12] and adsorption [13,14]. Adsorption is one of the useful techniques of removing selenium from wastewater due to the scientific advancement and cost advantages [15,16]. However, the key to its application is the adsorbent's effectiveness, which requires an adsorbent with a high density of binding sites per unit volume and a strong affinity to the adsorbate [17].

Nanoscale zerovalent iron (nZVI) is an extensively used nanomaterial adsorbent for reducing several organic contaminants because it has a large specific surface area and high reactivity [18]. It is also considered a cheap and eco-friendly reducing agent for adsorption [19–21]. nZVI has been used in treatment technologies for removing or degrading chemical contaminants such as chlorinated solvents [22], chlorinated pesticides [23], organophosphates [24], nitrosamines [18,25], nitroaromatics [22] and metalloids [26]. However, SeMet and SeCys (organoselenium) removal using nZVI adsorbent are limited due to the prevalent challenges that affect the adsorption performance and reactivity of nZVI in an aqueous medium. Recently, Okonji et al. [10] reported that in spite of the numerous advantages of nZVI, SeMet could not adsorb actively onto nZVI, while SeCys removal from wastewater was below 45% using nZVI technology.

The implementation of the zerovalent iron technology is often confronted with several challenges [27]. These include: (i) Easy oxidation and formation of a passivation layer, thereby reducing its reactivity and limiting its practical use [19,28]. (ii) The nZVI forms rapid corrosion when exposed to water, thereby passivating its surface and considerably deteriorating its contaminant alteration capability over time [29–31]. (iii) Agglomeration of particles [32,33]. Hence, techniques that can remove some of these limitations and enhance nZVI performance for SeMet and SeCys removal from waters are needed.

Immobilization of nZVI onto a supporting material, such as granular activated carbon (GAC), is a promising strategy to address some of the issues described above. Moreover, elemental iron (Fe^0) and GAC can form a Fe^0/GAC microelectrolysis system capable of enhancing the removal capacity of nZVI [34]. Though nZVI/GAC composites have been tested for the removal of nitrosamine compounds [18], arsenic from aqueous solution [15] and inorganic selenium treatment [35,36], no information is currently available on SeMet and SeCys adsorption onto nZVI/GAC. As far as we know, there is no publication on organoselenium removal using nZVI/GAC composites in the literature.

This study investigated the adsorption of SeMet and SeCys using nZVI/GAC composites. The objectives of the study were: (a) prepare nZVI/GAC composite and test the removal efficiency to adsorb SeMet and SeCys contaminants from wastewaters; (b) investigate the impact that several operational parameters including the adsorbent loading, pH, adsorbate initial concentrations and kinetics could have on the removal of organoselenium by nZVI/GAC; and (c) evaluate the effects of coexisting ions in organoselenium remediation. As far as we are aware, this is the first study to investigate the use of nZVI/GAC composites to remove organic selenium from wastewater.

2. Experimental Section

2.1. Chemicals

All chemicals used in this study were of analytical grade. SeMet (>98%) and SeCys (>98%) were acquired from TCI America. Ferrous sulfate heptahydrate ($\text{FeSO}_4 \cdot 7\text{H}_2\text{O}$, $\geq 99\%$) was supplied by T.J Baker, Germany. Hydrochloric acid (HCl) (>98%), sodium borohydride (NaBH_4 , $\geq 98.0\%$), polyethylene glycol-2000 (PEG-2000) and absolute alcohol ($\geq 99.7\%$) were purchased from Sigma-Aldrich Chemical Company (Burlington, MA, USA) and utilized in the synthesis of the nZVI. Powdered coconut-shell-based activated carbon (GAC, 12×40 mesh) was acquired from Calgon Carbon (Moon Township, PA, USA).

2.2. Synthesis of Iron Nanoparticle (nZVI)

The nZVI particles were synthesized following a liquid-phase reduction method described elsewhere [27]. A total of 7.0 g of $\text{FeSO}_4 \cdot 7\text{H}_2\text{O}$ was dissolved in 200 mL of an ethanol-deionized water solution (ethanol/water = 1:1 *v/v*), while PEG-2000 (0.52 g) was added as a dispersant to facilitate the reduction of nZVI aggregation in the ferrous sulfate solution. This was followed by the drop by drop addition of 100 mL of 1.0 mol/L NaBH_4 while the solution was constantly agitated at 300 r/min for 45 min with a magnetic stirrer (VWR 200 model) at ambient temperature. The chemical reaction is represented in Equation (1).



The synthesized nZVI particle was allowed to settle and was segregated from the liquid state using vacuum filtration apparatus. The solid particles were rinsed with water several times and dried at 60 °C. The experiment was conducted with continuous N_2 bubbling to prevent the synthesized nanoparticles from being passivated by oxygen.

2.3. Preparation of the nZVI/GAC Composite

Granular activated carbon was utilized as a support for nZVI particles. An amount of 10 g of dry GAC was washed and repeatedly rinsed with DI water, then soaked in 200 mL of ferrous sulfate solution with PEG-2000 for 3 h. Before the NaBH_4 solution was added in a dropwise manner, the slurry was initially stirred up in an ultrasonic bath for 2 h and stirred again for another 1 h under N_2 purging. The GAC-supported nZVI was segregated from the solution, labeled and vacuum dried at 60 °C and stored in a desiccator purged with N_2 . The process was similar to that of nZVI synthesis described above.

2.4. Characterization of Adsorbents

Adsorbent samples (nZVI/GAC) characterization was before and after the adsorption of organoselenium using SEM/EDS, XRD and BET analysis. The morphological properties of the synthesized nZVI/GAC adsorbent were obtained using a scanning electron microscope at 10–15 kV (SEM, ThermoFisher, Waltham, MA, USA, Quanta FEG 250), as shown in Figure 1. X-ray mapping and analysis were performed using a Bruker Quantax micro-analysis system, consisting of a Quantax 5030 SDD-type X-ray spectrometer, SVE III signal processing unit and Bruker Esprit v2.1 software. The XRD patterns (mineralogical properties) were collected with the aid of an X-ray diffraction instrument (Rigaku MultiFlex), and the diffraction angle 2θ in the range of 10–80° was used. The total pore volume and BET surface area were derived by the N_2 adsorption method at 77 K on a PMI Automated Brunauer-Emmett-Teller (BET), Quantachrome ChemBet (3000 CB-SCL).

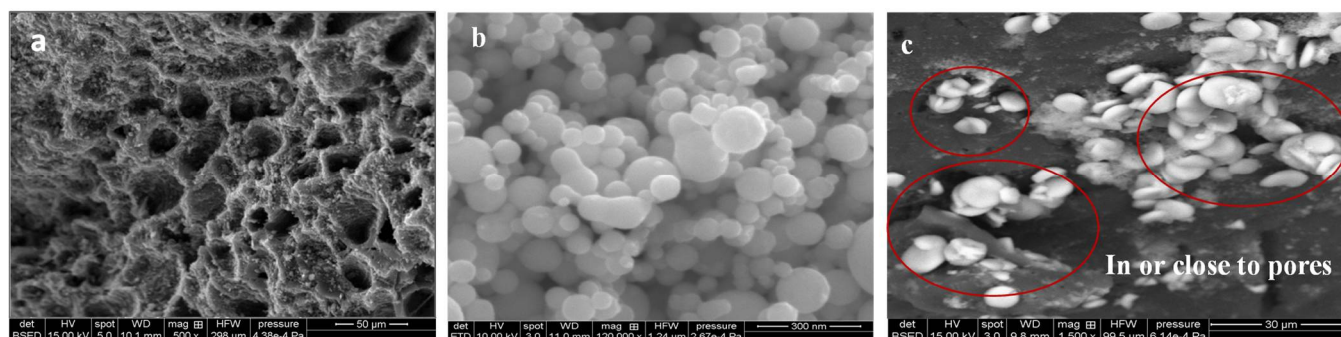


Figure 1. Cont.

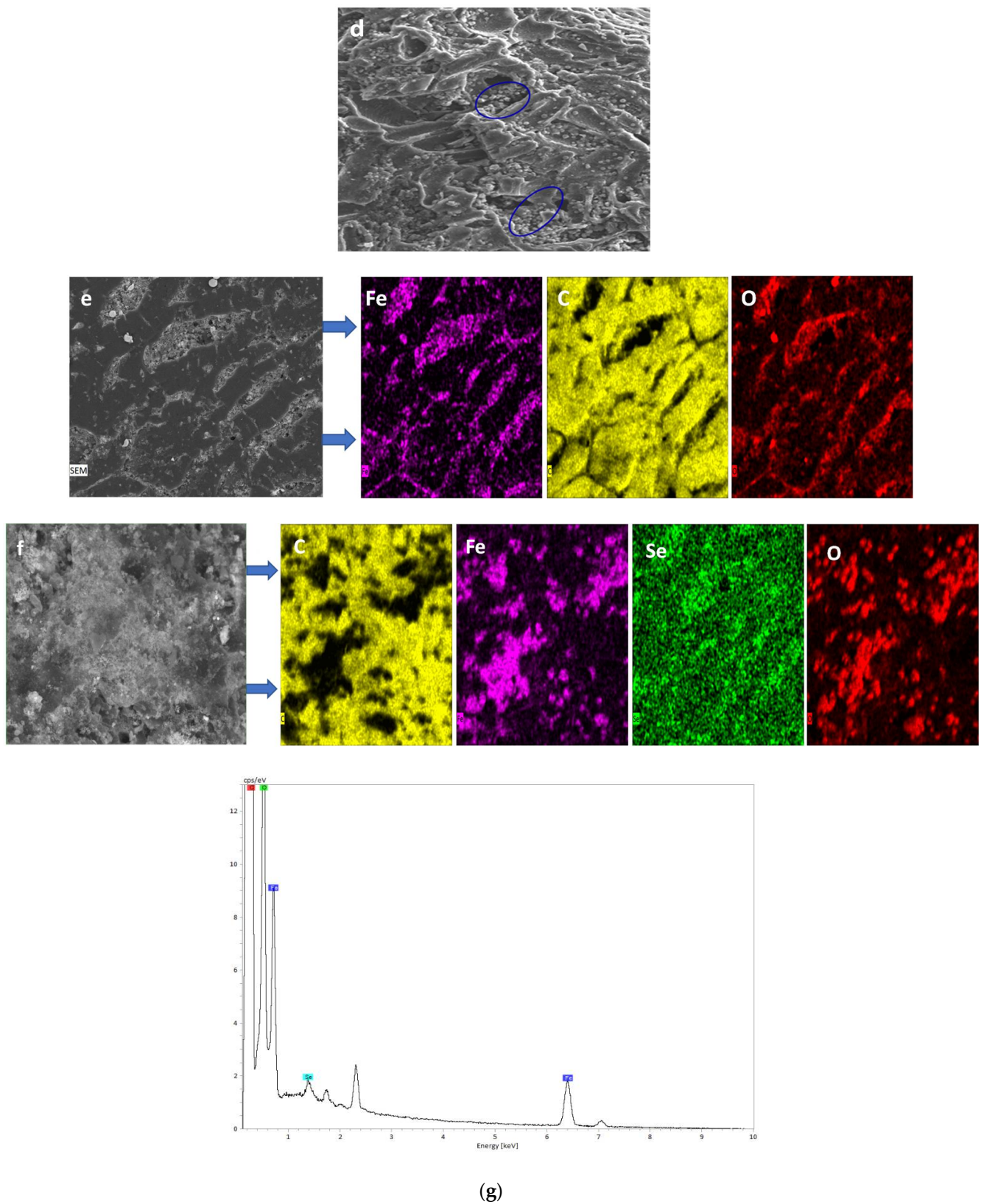


Figure 1. SEM images: (a) activated carbon, (b) non-supported nZVI, (c) nZVI/GAC composite, (d) nZVI/GAC post-adsorption. SEM images of energy-dispersive spectrum of nZVI/GAC: (e) pre-adsorption and (f) post-adsorption. (g) Energy-dispersive spectrum distribution plot of nZVI/GAC showing post-removal elemental composition (C, O, Fe and Se).

2.5. Batch Adsorption Studies

A stock solution of SeCys ($C_3H_7NO_2Se$) and SeMet ($C_5H_{11}NO_2Se$) (750 mg/L each) was prepared separately by dissolving of 0.5 g of each chemical in 250 mL of deionized water. The test solution was prepared by diluting the stock solution as appropriate. The concentration of SeMet and SeCys in the test solutions used for various parametric studies was 0.5 mg/L. All batch experiments were conducted using 150 mL straight-wall glass jars. The solutions were stirred using a magnetic stirrer (VWR 200 model), the mixtures were constantly agitated at a speed of 180 rpm in a temperature-regulated orbital shaker, and the experiment was performed at ambient temperature. 1 M of HCl or NaOH was added to alter the starting pH of the solution. At different time intervals, 10 mL aliquots of samples were periodically collected and instantly filtered using 0.22 μm PTFE syringe filter. The influence of pH on the adsorption of SeMet and SeCys was investigated by conducting experiments in the pH range of 3.0–12.0. For statistical reliability, the experiments were conducted in duplicate, the samples were analyzed in triplicate and the average results were presented. Standard deviation was used to evaluate the error bars analysis.

2.6. Analysis and Equipment

The overall selenium concentrations in the solutions were studied with an inductively coupled plasma optical emission spectrometer (ICP-OES) (Thermo Scientific icap 7000 series, Waltham, MA, USA). The limit of detection and quantitation for selenium was estimated as 0.005 and 0.01 mg/L, respectively. A digital pH device (VWR symphony B20PI) was used to measure the changes in pH of the system over time.

2.7. Adsorption Kinetics

Adsorption kinetics of SeMet and SeCys onto nZVI/GAC adsorbent was evaluated. The adsorbent dose was 3 g/L, which is the optimum dose obtained from dosage studies. The adsorption capacity q_e (mg/g) was calculated using the following equation:

$$q_e = \left[\frac{(C_0 - C_e)}{m} \right] \times V \quad (2)$$

where C_0 represents the initial concentration (mg/L) and C_e the equilibrium concentration (mg/L); M is the mass of the adsorbent (g); and V is the volume of the solution (L). PFO model was evaluated using the equation below:

$$q_t = q_e \left(1 - e^{-kt} \right) \quad (3)$$

where q_e and q_t (mg/g) represent the amount of adsorbate adsorbed at equilibrium and at time (t), respectively, and k (min^{-1}) is the rate constant. A pseudo-second-order kinetic model was applied to the kinetics data using Equation (4):

$$\frac{t}{q_t} = \frac{1}{k_2 q_e^2} + \frac{t}{q_e} \quad (4)$$

where k_2 is pseudo-second-order kinetic rate constant ($\text{g mg}^{-1} \text{min}^{-1}$) and adsorption time (min). The initial adsorption rate h of the system is equal to $k_2 q_e^2$ ($\text{mg g}^{-1} \text{min}^{-1}$).

2.8. Adsorption Isotherm Studies

Adsorption isotherms were obtained at various initial concentrations (0.0156 to 1 mg/L) for SeMet and SeCys. The adsorption mechanism (multilayer versus monolayer) was evaluated using Freundlich and Langmuir isotherm models [37,38]. The Freundlich model

explains the relationship between the equilibrium concentration and the adsorption capacity. This is illustrated with Equation (5) [37]:

$$\frac{(C_0 - C_e)}{M} V = K_f C_e^{\frac{1}{n}} \quad (5)$$

where C_e is the equilibrium concentration (mg/L), C_0 means initial concentration (mg/L), M represents adsorbent mass (g), V represents the volume of the solution (L), K_f and n are Freundlich parameter constants. Equation (6) presents the mathematical illustration for Langmuir isotherm [38].

$$q_e = q_m K_c \frac{C_e}{1 + K_c C_e} \quad (6)$$

where q_e represents equilibrium (mg/g) adsorption capacity, q_m (mg/g) means maximum adsorption capacity, the equilibrium adsorption constants are given as K_c (L/mg) and C_e means equilibrium concentration (mg/L). The premise that adsorption takes place at a limited specific localized site (monolayer) explains Langmuir isotherm [38]. Moreover, the Langmuir model can be further evaluated using Equation (7) [17].

$$R_L = \frac{1}{1 + K_c C_0} \quad (7)$$

An adsorption process is said to be irreversible when $R_L \sim 0$, favorable when $1 > R_L > 0$, unfavorable when $R_L > 1$ and linear when $R_L \sim 1$ [17].

2.9. Effect of Competing Ions

The effect of competing ions on the adsorption of organoselenium onto nZVI/GAC was investigated. Some common anions (sulfate, carbonate, nitrate, phosphate) and cations (calcium, magnesium, ferrous, potassium) which are frequently encountered in water and wastewaters were selected for interference evaluation. The molar proportion of the added ions to organoselenium was 200:1.0. A solution of 100 mL comprising organic selenium and coexisting ions was mixed with 0.3 g of synthesized GAC-supported nZVI after pH adjustment and allowed to equilibrate for a maximum contact time of 24 h.

2.10. nZVI/GAC Regeneration

Regeneration of nZVI/GAC composite was conducted to ascertain its reuse capabilities. After SeCys and SeMet adsorption using 0.3 g nZVI/GAC with 100 mL solution for 6 h, the nZVI/GAC particles were separated from the treated solution by vacuum filtration and washed with DI water to expunge any organoselenium that was not adsorbed (the process involved mixing nZVI/GAC with NaOH and agitate in a temperature-controlled orbital shaker). The adsorbent was then desiccated overnight under a vacuum at 25 °C (room temperature) and utilized for the next experiment.

3. Results and Discussion

3.1. Pre- and Post-Adsorption Characterization of nZVI/GAC

Figure 1 presents the SEM images of GAC, synthesized non-supported nZVI and nZVI/GAC composite pre and post organoselenium removal. It also presents the dispersive energy spectrum (EDS) analysis of nZVI/GAC pre and post adsorption. From Figure 1a, there is a lack of uniformity in the pore distribution of GAC, as well as a variance in the pore sizes. Figure 1b reveals that the synthesized non-supported nZVI particles are spherical, with sizes ranging from 60–120 nm and clustered into irregular chain-like shapes. The build-up of the nZVI particles is related to magnetic forces, electrostatic interaction [39–41] and van der Waal force [42]. As depicted in Figure 1c, some obvious spherical particles with a size of about 40 nm were visible on the surface, cracks, or inside the GAC pores in a chain-like shape. This is an indication that the nZVI was successfully supported or loaded onto the GAC [43]. Embedding nZVI into GAC pores is an important

phenomenon that aids adsorbent regeneration and is reused in water treatment facilities without losing the iron nanoparticles [15]. Compared with the SEM image of Figure 1b, the reduction in the nZVI/GAC particle size is because GAC can stabilize and disperse nZVI particles, thereby inhibiting aggregation of nZVI. Similar findings have previously been reported elsewhere [43]. The reactivity of GAC-supported nZVI is an advantage that comes from the small size of the supported nZVI particles, resulting in a higher number of reactive regions (adsorption sites) on the surface [44]. However, the occurrence indicated by blue circles observed in Figure 1d shows that the GAC-supported nZVI particles are clustered and interconnected after the withdrawal of the organoselenium, which was consistent for the removal of both SeCys and SeMet. Furthermore, Figure 1e shows that the dispersive energy spectrum of nZVI/GAC consists of carbon (C), iron (Fe) and oxygen (O). This phenomenon demonstrates that the nZVI particles are immobilized on GAC surface, which is partially oxidized [44]. Similarly, the mapping of EDS image of nZVI/GAC after the organoselenium removal (Figure 1f) and EDS distribution plot after organoselenium removal (Figure 1g) demonstrated the presence of C, Fe, O and Se at the surface. The EDS results indicate that selenium is adsorbed on the surface of nZVI/GAC composite, which points to the adsorbent (nZVI/GAC) being oxidized after adsorption [44].

Textural structure and iron content analysis data of GAC and nZVI/GAC are shown in Table 1. S_{BET} and V_{BJH} are $794.00 \text{ m}^2/\text{g}$ and $0.07 \text{ cm}^3/\text{g}$, respectively. The data show that both were significantly lower than those of the raw GAC ($1078.70 \text{ m}^2/\text{g}$ and $0.10 \text{ cm}^3/\text{g}$), showing a significant block on GAC pores by nZVI particles. Figure 2 illustrates the N_2 adsorption-desorption isotherms; clearly, the isotherm curves showed two hysteresis loops, which indicates the presence of two-pore systems in both GAC and nZVI [17,43,45]. In general, Table 1 and Figure 2 show that the decrease in pore volume and the centered pore size suggest that the nZVI particles were successfully loaded inside GAC pores [17].

Table 1. Textural structure parameters of GAC and nZVI/GAC.

Sample	S_{BET} (m^2/g)	V_{BJH} (cm^3/g)	Pore Size (nm)
GAC	1078.70	0.10	4.63
nZVI/GAC	794.00	0.07	3.42

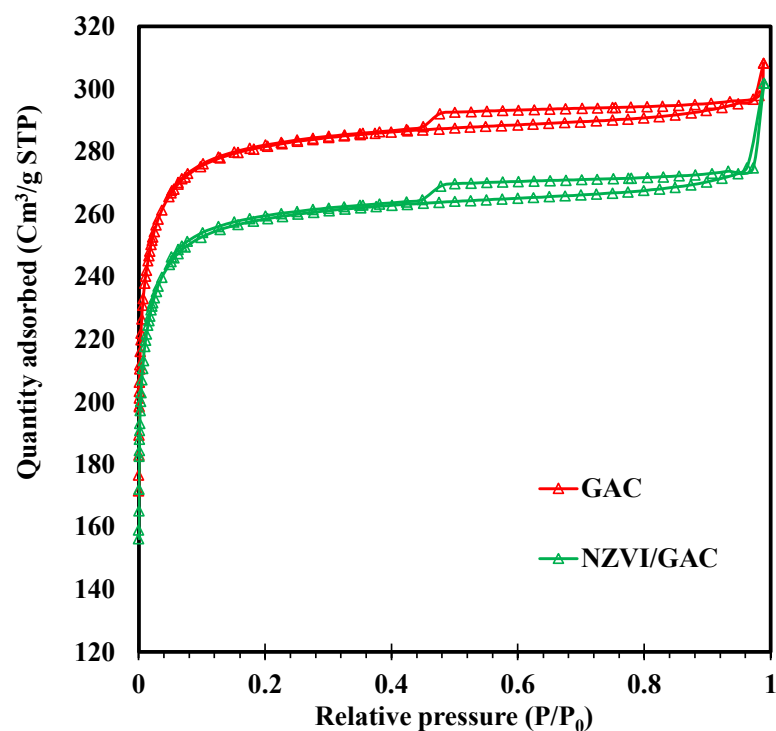


Figure 2. Nitrogen adsorption–desorption isotherms of GAC and GAC-supported nZVI.

The XRD patterns of GAC, nZVI and nZVI/GAC are illustrated in Figure 3. As shown, the peaks of nZVI are well indexed as ferrites, of which diffraction angle 2θ at 44.64° and 65.0° are suggestive of (110) and (200) for $\alpha\text{-Fe}^0$ crystal planes, correspondingly. This observation shows that unsupported nZVI has high purity and a good crystallographic degree [42,46]. For GAC, two broad peaks at 2θ ($22.5\text{--}24.3^\circ$ and $42.7\text{--}43.9^\circ$) were observed, which corresponds to the peculiarity of amorphous carbon [44,47]. For nZVI/GAC, the recurrence of the broad peaks indicates that GAC structures are not destroyed after nZVI immobilization [43].

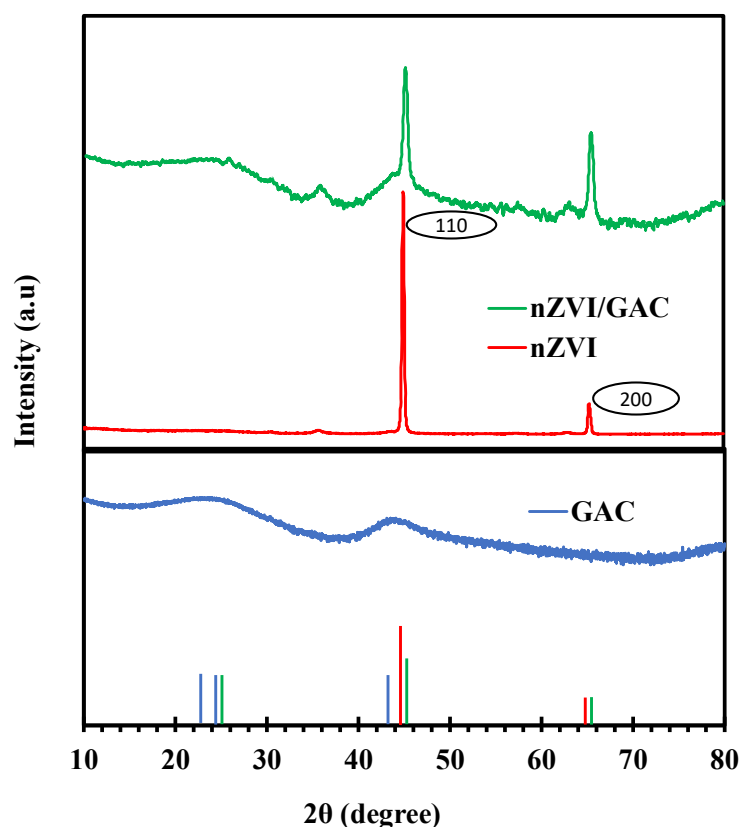


Figure 3. XRD analysis of GAC-synthesized-nonsupported nZVI and GAC-supported nZVI.

3.2. Adsorption of Organic Selenium by nZVI and nZVI/GAC Composites

The removal capacity of organoselenium by nZVI and nZVI/GAC is presented in Figure 4. In comparison, higher capture capacity was observed with GAC-supported nZVI particles, as opposed to the minimal uptake capacity by nZVI. Approximately 59.2% and 10.8% removal were achieved for SeCys and SeMet by nZVI after 6 h, whereas about 97.2% and 64.9% of SeCys and SeMet were removed by nZVI/GAC composite. Significantly, a higher removal capacity of organoselenium was observed with the synthesized composite. The low performance of nZVI is attributed to the easy oxidation and clustering of nZVI particles, affecting the adsorption and its reduction capability of organic contaminants in the Fe^0 system [18,29]. In an aqueous medium, when Fe^0 is exposed to moisture and oxygen, aerobic corrosion occurs and the Fe^0 is oxidized to ferrous ions [12]. It is known that ferrous ions can easily form ferric ions through oxidation and thereafter form loose ferric hydroxide/oxide layer (film) in water as by-products of corrosion [48,49]. The oxide layer (eg., Fe_2O_3) can result in passivation, reducing the reactivity of iron or its reaction capability [50]. This phenomenon explains the nZVI adsorption process [51] as well as the method of removal for organoselenium by nZVI [10].

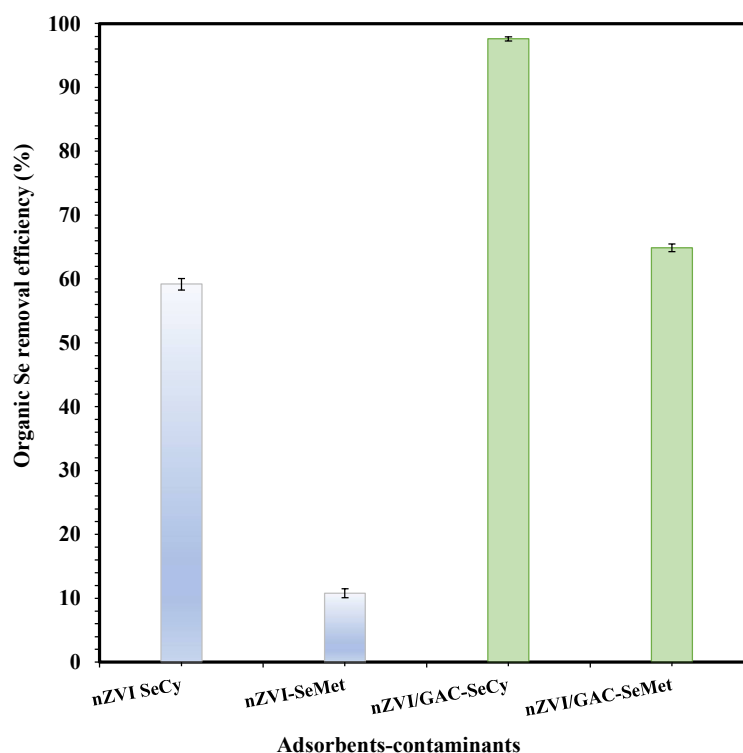


Figure 4. Compare adsorption capacity of synthesized nZVI and nZVI/GAC for removal of SeCys and SeMet from aqueous solution: Organic selenium initial concentration 0.5 mg/L, adsorbent ratio 3 g/L, pH 7.0, at 25 °C for 6 h period.

The BET analysis showed that nZVI has a small surface area of relatively less than 25 m²/g. However, achieving a higher uptake capacity will require a large surface that can necessitate more binding sites to create a stronger affinity with adsorbate [17]. In this instance, nZVI surface area is limited and can undoubtedly contribute to low adsorption performance.

Contrarily, the higher adsorption capacity observed with nZVI/GAC composites for the removal of SeCys and SeMet resulted from the fact that there are more available adsorption sites on nZVI/GAC due to the higher surface area (794 m²/g), which is rich in micropores [18]. In the C-Fe⁰ micro-electrolysis reaction system, organoselenium can partition onto nZVI/GAC surface. Fe⁰ formed microscopic galvanic cells and activated carbon facilitated the corrosion of Fe⁰, which accelerated the electron transfer between nZVI and GAC [52]. This reaction process can enhance the removal capability of nZVI/GAC [18,52,53].

The preferential adsorption of SeCys over SeMet is evident in Figure 4. SeCys more readily partitions onto the adsorbent's surface, irrespective of the adsorbent. A similar finding with a detailed explanation has been reported in a previous study by Okonji et al. [10]. SeMet is an analogue of methionine, which does not interact actively with the metal surface; hence, SeMet is more refractory to adsorption than SeCys, which is an analogue of cysteine [10,54].

3.3. Adsorbent Dosage

Figure 5a,b shows the result of nZVI/GAC dosage studies for removing organoselenium from wastewater via batch experiment at pH 7.0 and initial concentration of 0.5 mg/L. The removal rate of both SeCys and SeMet appears to increase with an increase in the nZVI/GAC dosage. This is because a positive effect is exerted on nZVI/GAC adsorption capacity due to the corresponding rise in the number of active sites and the reactive surface area [55]. For an adsorbent dose of 2–7 g/L, more than 97% of SeCys was swiftly removed

within 4 h, and equilibrium was achieved in 3 h. SeMet adsorption increased from 50.6% to 68.1% when the nZVI/GAC dosage applied increased from 1 to 7 g/L. However, the rate of removal between 3–7 g/L was less than 5% for SeMet adsorption; for SeCys, no change in adsorption was observed between 3 and 7 g/L after 4 h, indicating that 3 g/L is an optimum dosage for organoselenium removal by nZVI/GAC. Clearly, for a dose of 1 g/L, adsorption of SeCys and SeMet was progressive; however, the solution did not attend equilibrium in 6 h, indicating that the uptake was slower. Overall, the adsorbent large surface area enhanced the adsorption capacity of the adsorbent as a result of more active adsorption sites, which consequently leads to a higher removal rate [10,21,56].

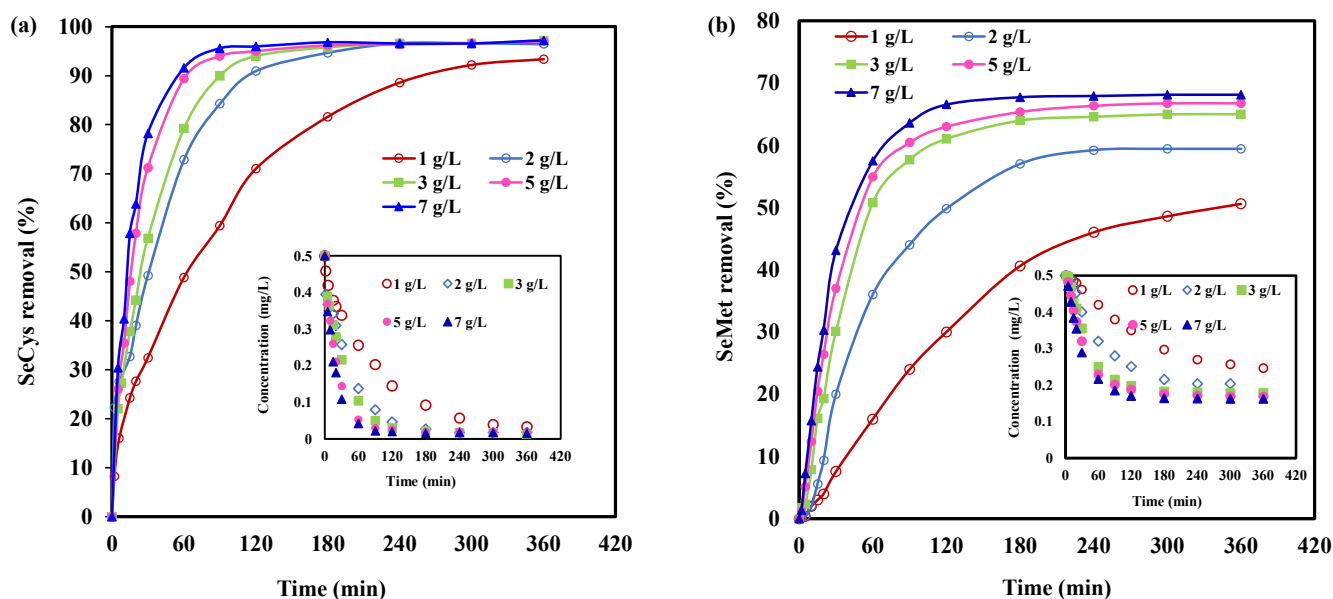


Figure 5. Dosage studies on removal of organic selenium by nZVI/GAC: (a) SeCys and (b) SeMet: (initial concentration of 0.5 mg/L, pH 7.0, at 25 °C). Contact time 6 h.

3.4. Effect of pH

The pH of a solution is an important factor that can influence the adsorption process, surface functional groups and the interaction between the adsorbent and adsorbate. In this research, the effect of pH on the removal of organoselenium by nZVI/GAC was investigated by changing the pH of the solution over a range of 3–12 (see Figure 6). As observed in Figure 6, the concentration of SeCys and SeMet adsorbed by nZVI/GAC increased slowly with an increase in the pH from 3.0 to 7.0. A decrease in the removal efficiency from 92.0% to 46.0% for SeCys, and 59.4% to 22.0% for SeMet, was observed when pH was further increased from 8.0 to 12. These shifts are due to the formation of oxide coatings at greater pH values (>8), which hinders the oxidization of Fe^0 to Fe^{2+} [57] and the electro-repulsion effect. These factors can result in a reduction of the adsorption capacity of nZVI/GAC.

The point of zero charges (pHpzc) of nZVI/GAC is reported as 3.2 [58], which indicated that the surface carries a positive charge at pH values below pHpzc (attracts anions) and carries a negative charge at high pH (repels anions) [58]. This interdependence between the surface charge and molecular charge facilitates the adsorption of molecules to take place on the surface of nZVI/GAC. Moreover, SeCys and SeMet are zwitterions (with carboxyl groups and amino groups). The isoelectric points (Ip) are 5.54 for SeCys and 5.75 for SeMet [59,60]. Hence, it is expected that SeMet is protonated at lower pH (i.e., <5.75) which means positively charged and deprotonated at higher pH (i.e., >5.75) negatively charged [61]. The same phenomenon applies to SeCys.

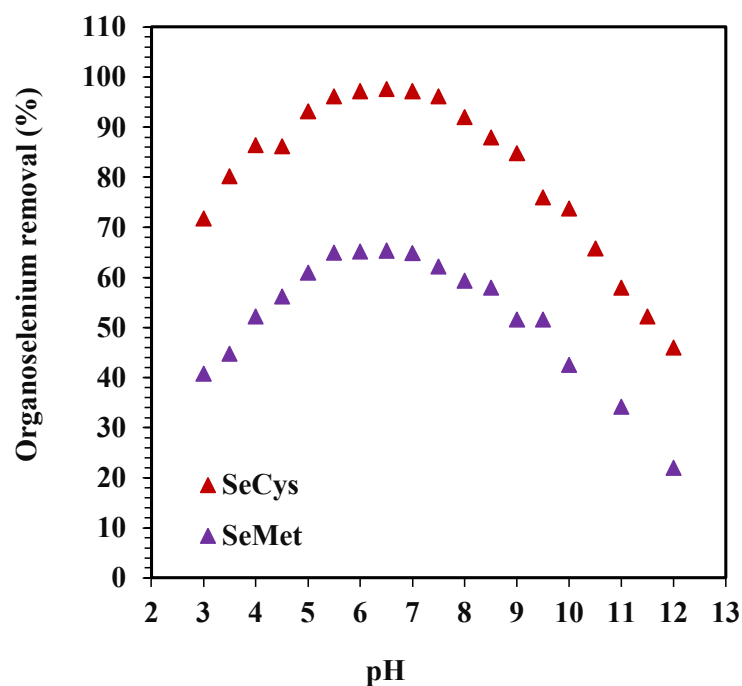


Figure 6. Adsorption envelopes of SeMet and SeCys on nZVI/GAC at initial organoselenium concentration of 0.5 mg/L and adsorbent ratio of 3 g/L. Contact time: 24 h at 25 °C.

Conversely, at the $\text{pH} < 3.2$, the surface charge of nZVI/GAC would behave as a positive charge and that of organoselenium species would also carry a positive charge [61,62]. Therefore, because of forces of repulsion between similarly charged molecules, the removal efficiency was reduced (not as high as that of a near-neutral pH range). Similarly, when the solution pH is higher than 5.75 (or 5.54 for SeCys), then the organoselenium species and nZVI/GAC will be negatively charged, resulting in a repulsion effect. Between pH 3.2 and 5.75, organoselenium would be positively charged and nZVI/GAC negatively charged. This will lead to electrostatic interaction between organoselenium species and nZVI/GAC; hence, substantial removal was achieved [61]. However, at near-neutral pH, higher attraction occurred which resulted in maximum removal. Two factors may be responsible for the high adsorption: (i) the prompt dissolution of the oxides on the surfaces of nanoparticles and (ii) the unlocking of the active sites which can accelerate iron corrosion reaction [61,62]. Overall, electrostatic force controls SeCys and SeMet adsorption by nZVI/GAC.

3.5. Initial Concentration Studies

The effects of initial concentration (C_0) on organoselenium removal from contaminated water by nZVI/GAC are shown in Figure 7. Initial concentrations of 0.25, 0.4 and 1 mg/L at pH 7.0 were used for this study. As summarized in Table 2, nZVI/GAC adsorption capacity (q_e) increased with higher C_0 , irrespective of the contaminant. It stands to reason that the increase in C_0 provided the required energy needed to overcome the mass transfer resistance between the adsorbate and adsorbent [18]. The removal efficiency obtained for SeCys were 99.6, 98.3, 90.3 and 72.8%, 69.5%, 60.2% for SeMet, corresponding to C_0 defined above, respectively. Because nZVI/GAC amount (quantity) was fixed and the available adsorption sites were unchanged, the reaction of the composites reduces with time [18]. This explains the reduction in removal efficiency observed at higher concentrations [18]; another study ascribed the same phenomenon to reaction and surface-mediated action (higher concentration hindered the reaction) [63].

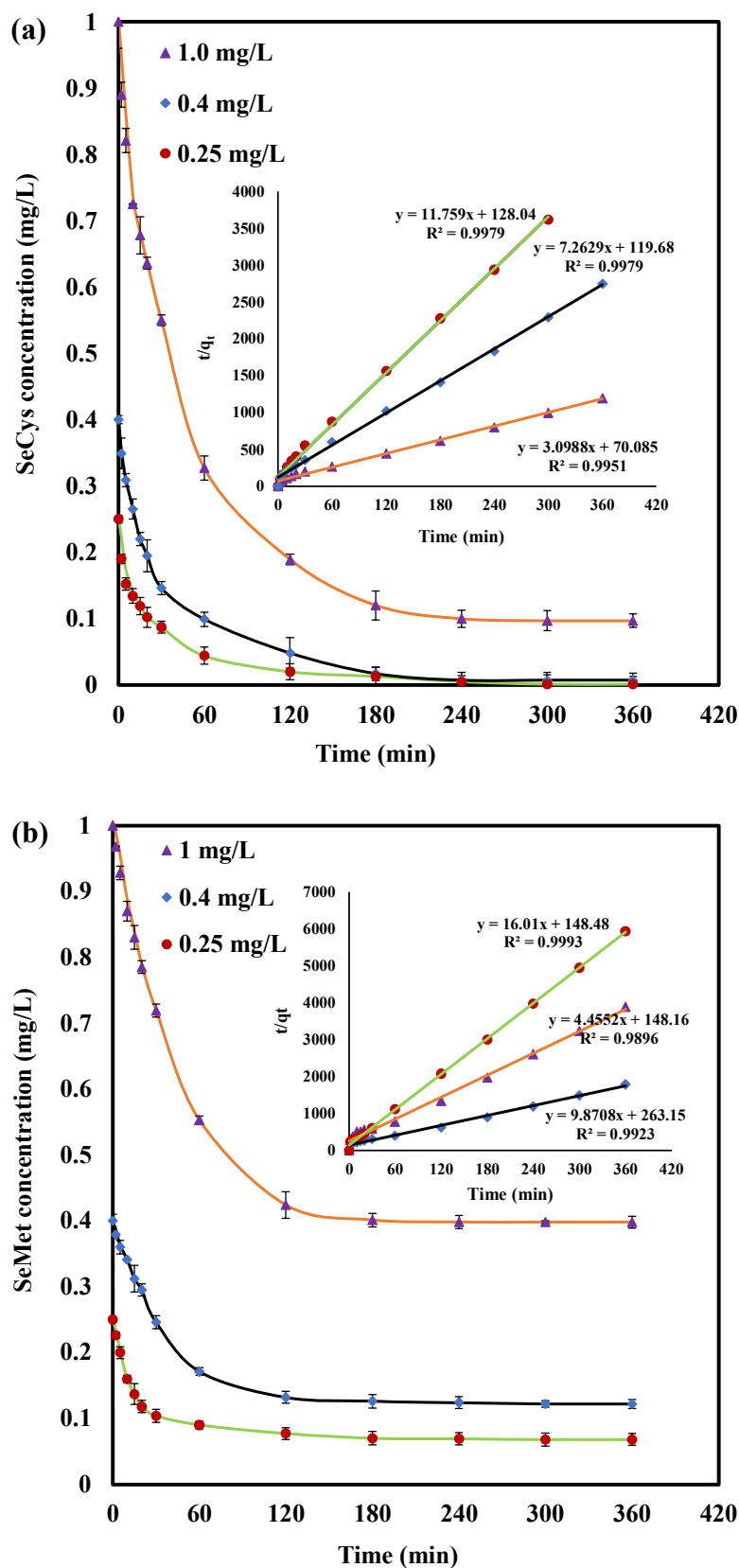


Figure 7. Effect of initial concentration: (a) SeCys and (b) SeMet: Initial concentration 1.0, 0.4 and 0.25 mg/L (all experiments were conducted at pH 7.0, 3 g/L of nZVI/GAC and 25 °C).

Table 2. Key parameters on effects of initial SeCys and SeMet concentration adsorption onto nZVI/GAC.

Parameter	SeCys			SeMet		
C_o (mg/L)	0.25	0.4	1	0.25	0.4	1
q_e (mg.g ⁻¹)	0.085	0.138	0.323	0.0607	0.101	0.224
K_2 (g mg ⁻¹ min ⁻¹)	1.059	0.441	0.137	1.726	0.370	0.134
R^2	0.998	0.998	0.995	0.999	0.992	0.989

The kinetic equations were employed to validate the experimental data to evaluate the potential rate-limiting steps associated with the adsorption processes. PSO kinetic model describes the data depicted in Table 2 adequately; the inset of Figure 7 (linearization plot) shows the fitted data. The correlation coefficients (R^2) obtained were higher than 0.99 for all the concentrations studied. The rate constant (K_2) ranges from 1.059 to 0.137 g mg⁻¹ min⁻¹ for SeCys and 1.726 to 0.134 g.mg⁻¹.min⁻¹ for SeMet, respectively. Furthermore, the results show a decrease in K_2 with increasing organoselenium concentration. The corresponding decrease in K_2 was due to the longer duration and the solution required to reach equilibrium; a similar occurrence has been described in previous research [10,14,64,65].

3.6. Adsorption Isotherm

The equilibrium adsorption isotherms of organoselenium removal by nZVI/GAC are presented in Figure 8. Langmuir and Freundlich isotherm models describe the results summarized in Table 3. Figure 8a illustrates the adsorption isotherm for SeCys removal, which is best characterized by the Langmuir model. As stated in Table 3, the correlation coefficient corresponding to ($R^2 > 0.990$) explains that the Langmuir model is a better fit, which suggests that the uptake of SeCys is monolayer and it occurred at specific sites [66,67]. The maximum uptake capacity for Langmuir parameter q_m is 1.02 mg/g. The dimensionless constant is $R_L = 0.052$, which implies favorable adsorption isotherm and suitability of nZVI/GAC for SeCys removal [17,53].

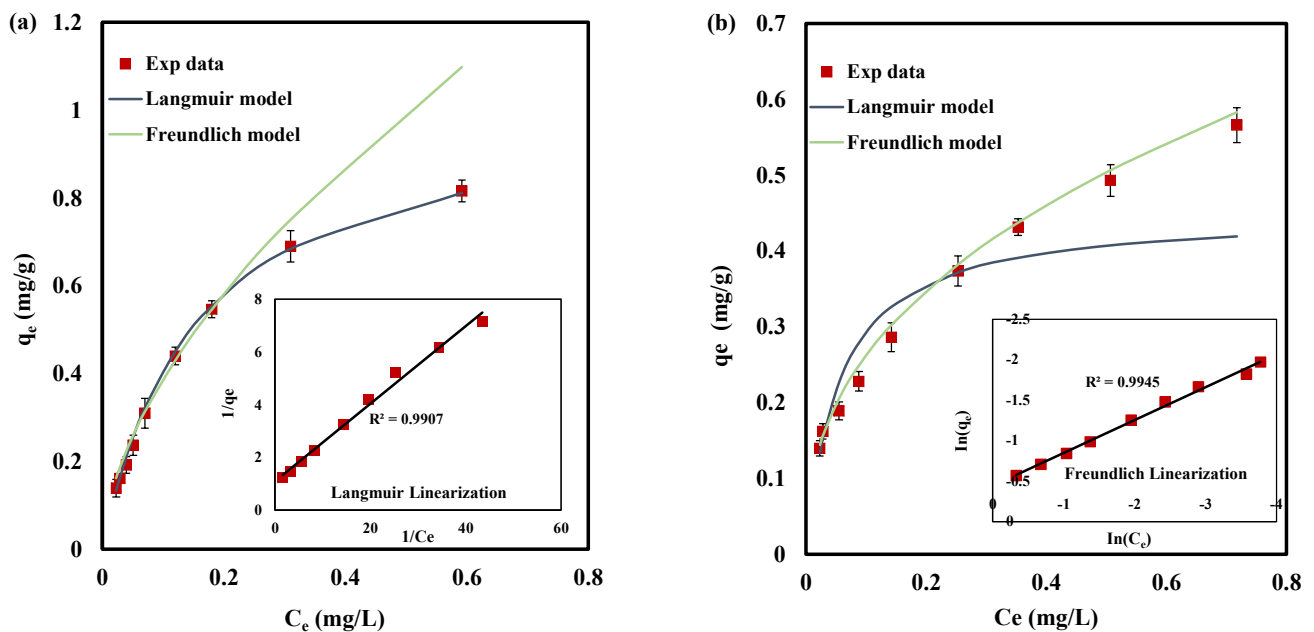


Figure 8. Isotherms result for organoselenium using nZVI/GAC composite. (a) SeCys; (b) SeMet. (The solid lines illustrate model fits; inset shows linearization fits.) Contact time: 24 h, pH 7.0, at 25 °C.

Table 3. Adsorption isotherm parameters for organoselenium removal.

	Langmuir Model			Freundlich Model		
	q_m (mg/g)	Kc (L/mg)	R^2	K_f	n	R^2
SeMet	0.45	18.37	0.919	0.67	2.46	0.994
SeCys	1.02	6.55	0.990	1.49	1.69	0.976

On the other hand, Figure 8b suggests that Freundlich model was a better fit than the Langmuir model for analyzing SeMet adsorption data. A higher correlation coefficient ($R^2 > 0.994$) for the Freundlich model indicates multi-layered adsorption of SeMet [10]. The Freundlich constant K_f relates to the adsorption capacity, which was evaluated to be 0.67. As depicted in Table 3, the adsorption intensity (n) was obtained as 2.46, implying a mildly rising isotherm curve and favorable adsorption [68], which is far greater than that previously reported [10].

3.7. Kinetics Studies

Figure 9 shows the adsorption kinetics study of SeCys and SeMet removal by nZVI/GAC. The result illustrates a two-step adsorption process: a fast initial adsorption stage (as adsorption occurs at the sites in the macropores), followed by a much slower process as the organoselenium adsorption approached equilibrium. The slow adsorption process observed after about 1 h into the experiment was caused by the reduced number of GAC surface sites around the nZVI particle [18] and due to the slower diffusion into the micropores in the composite. Approximately 97.6 and 64.9% of SeCys and SeMet, respectively, were removed in 6 h, and adsorption equilibrium was reached in 3 h. Pseudo-first-order (PFO) and pseudo-second-order (PSO) kinetics models (inset of Figure 9) were employed in evaluating the kinetics data. The rate constant (K_1 and K_2) values and the maximum adsorption capacity (q_e) for SeMet and SeCys are depicted in Table 4. The PSO model was a good fit for the kinetic data corresponding to correlation coefficients for SeCys ($R^2 > 0.998$) and SeMet ($R^2 > 0.999$). The adsorption capacity (q_e) values calculated by PSO forecasted that the removal process of organoselenium followed the PSO kinetic equation, proposing the dominance of chemical adsorption [53].

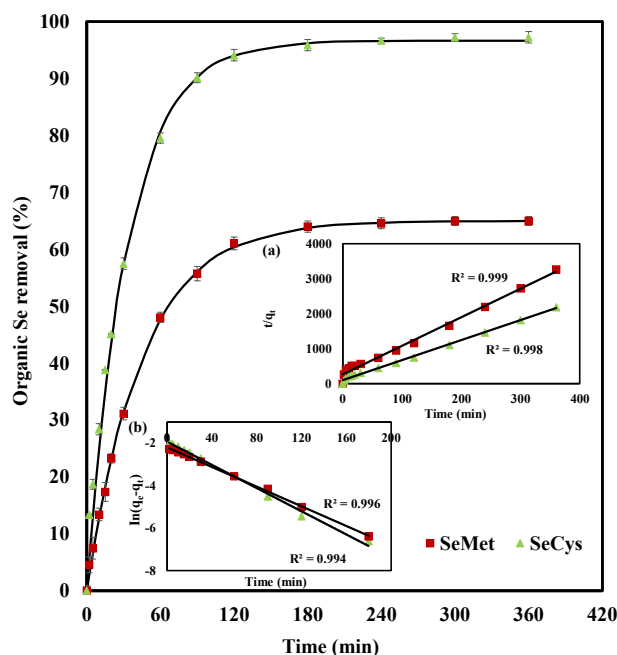


Figure 9. Organic selenium adsorption kinetics onto nZVI/GAC: (a) PSO and (b) PFO. Initial concentration 0.5 mg/L, 3 g/L, pH 7.0. (The solid lines illustrate model fits; inset shows linearization fits.)

Table 4. PSO and PFO kinetic data for SeCys and SeMet adsorption by nZVI/GAC.

Kinetic Parameter	SeCys	SeMet
nZVI/GAC		
Pseudo first order		
q_e (mg g ⁻¹)	0.161	0.110
K_1 (min)	0.030	0.022
R^2	0.995	0.996
Pseudo second order		
q_e (mg g ⁻¹)	0.173	0.122
K_2 (g mg ⁻¹ min ⁻¹)	0.314	0.252
h (mg g ⁻¹ min ⁻¹)	0.008	0.004
R^2	0.998	0.999

Conversely, the initial adsorption rate (h) data, displayed in Table 4, revealed a faster adsorption rate in SeCys compared to SeMet. The h value of SeCys is about twice that of SeMet, indicating SeCys has a much faster removal rate. The observance of a faster removal rate of SeCys as compared to SeMet in this research was consistent with earlier studies [10].

3.8. Effect of Ions Present in Water

The effects of some common anions (SO_4^{2-} , CO_3^{2-} , NO_3^- , PO_4^{3-}) and cations (Ca^{2+} , Mg^{2+} , Fe^{2+} , K^+) on organoselenium removal by nZVI/GAC were investigated. As shown in Figure 10, each ion competed distinctively with SeMet and SeCys adsorption to various degrees. Among the oxyanions investigated in this study, carbonate and phosphate were the most competitive oxyanions that reduced SeMet (40.7%, 53.0%) and SeCys (41.9%, 55.3%) removal efficiency, respectively. Sulfate ion also significantly decreased organoselenium removal by approximately 55.7% for SeMet and 88.9% for SeCys. These anions tend to form inner-sphere complex and weak bonds with iron oxides surfaces [15,69] and can easily be released [36,70]. Therefore, the oxyanions would compete for similar binding sites, thereby decreasing the adsorption of organoselenium. Nevertheless, the result shows that the existence of nitrate did not substantially impact SeMet and SeCys removal.

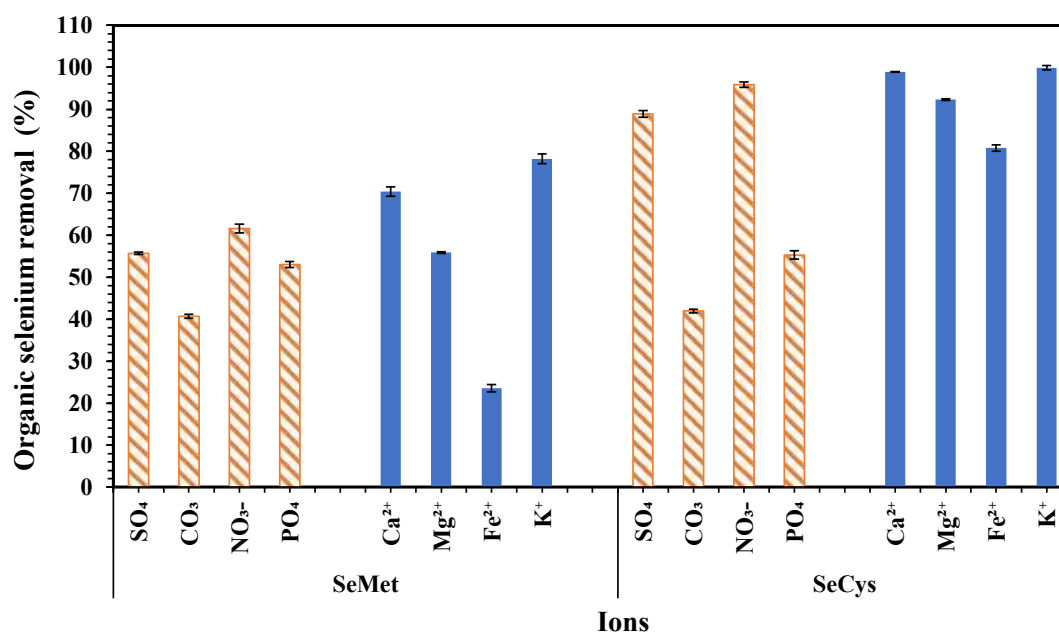


Figure 10. Effects of ions competing individually on organoselenium removal by nZVI/GAC with initial concentration of 0.5 mg/L, 3 g/L, pH 7.0 at 25 °C. The concentration of ions in the solution is 100 mg/L and contact time of 24 h.

Divalent metal cations such as Ca^{2+} , Mg^{2+} , Fe^{2+} and K^{+} have been reported to improve nZVI performance because these cations can serve as electron donors, enhance electron transfer, form bimetallic systems and de-passivate aged Fe^0 [18,19,71–73]. In this study, while Ca^{2+} and K^{+} increased the adsorption of SeMet (70.4%, 78.2%) and SeCys (98.9%, 99.9%) by nZVI/GAC, respectively, Mg^{2+} and Fe^{2+} were found to substantially suppress the removal efficiency of both SeMet (55.8%, 23.5%) and SeCys (92.3%, 80.7%). The weak adsorption experienced due to the presence of Mg^{2+} is because magnesium ions deteriorated the nZVI performance by shielding the reactive sites on the Fe^0 surface through precipitation [18]. On the other hand, the unfavorable effect of ferrous iron can be credited to the formation of complexes with organoselenium; consequently, the level of deprotonation/dissociation is suppressed and adsorption is decreased [15].

To further understand the effect of competing ions on organoselenium removal by nZVI/GAC, a comparative study of SeCys and SeMet removal in the presence of a group of cations and anions was evaluated. As shown in Figure 11a,b, anions (comprising SO_4^{2-} , CO_3^{2-} , NO_3^- , PO_4^{3-} , competing together) were observed to have more adverse effects on both SeMet and SeCys removal by nZVI/GAC compared to cations (Ca^{2+} , Mg^{2+} , Fe^{2+} , K^{+} , competing together in water). The result shows that the nZVI/GAC adsorption capacity for SeCys removal decreased from 0.159 mg/g to 0.104 mg/g because of the competing effect of the cations and 0.077 mg/g as a result of anions competing effect, after 3 h. The adsorption capacity also decreased from 0.106 mg/g to 0.084 mg/g (cations) and 0.037 mg/g (anions) for SeMet removal. The inhibitory effects of the cations were less compared to the anion. This is because metal cations in the solution would increase the surface charge of the adsorbent (nZVI/GAC). As a result, the cations have less inhibition and the removal efficiency is better [15].

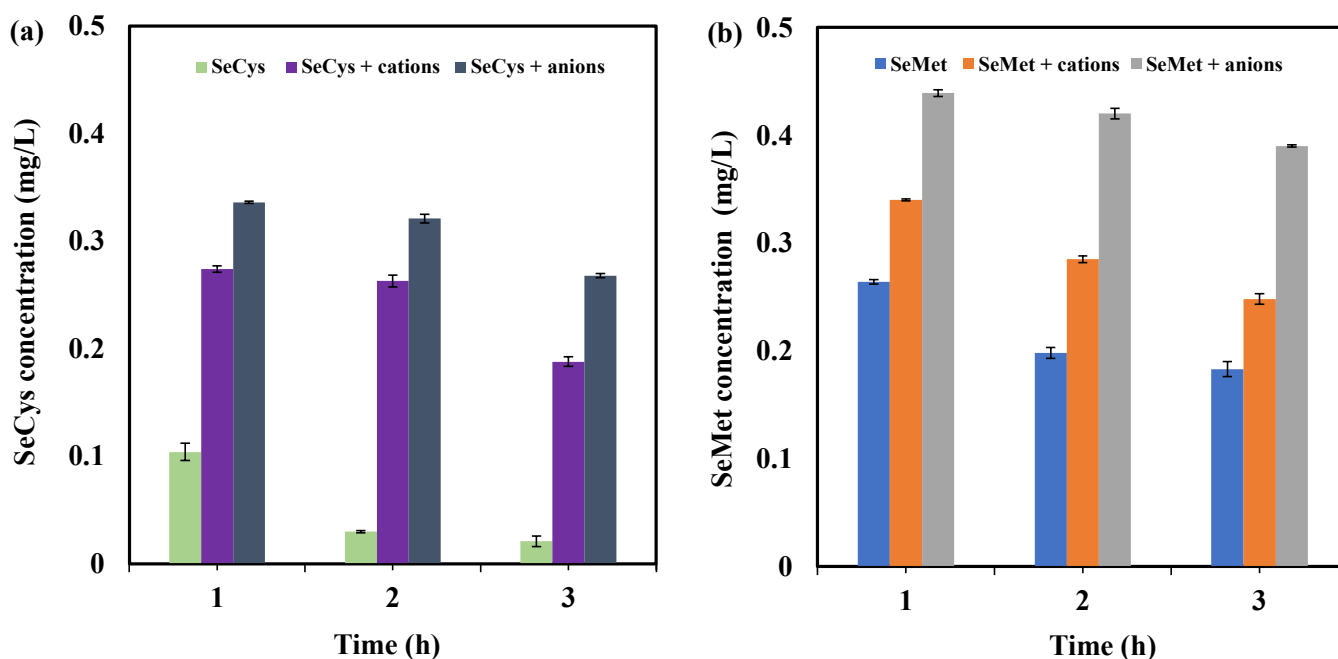


Figure 11. Comparative study on the influence of cations (competing together) and anions (competing together) on organoselenium removal by nZVI/GAC. (a) SeCys, (b) SeMet; initial concentration of 0.5 mg/L, 3 g/L, pH 7.0 at 25 °C. Contact time is 3 h; ion concentration is 100 mg/L.

3.9. NZVI/GAC Composite Regeneration and Reusability

The use of nZVI/GAC for organoselenium removal from wastewater is dependent on both its adsorptive capacity and regeneration for further use; hence, reusability of the as-synthesized nZVI/GAC was investigated. The results in Figure 12 show that nZVI/GAC could be regenerated, retaining a promising 92.8% of SeCys and 57.7% of SeMet removal

efficiency after six cycles. NZVI/GAC adsorption performance did not reduce substantially at the end of the last cycle, showing that the synthesized nZVI/GAC was mechanically and chemically robust [15] and can treat SeCys and SeMet effectively. Some of the advantages of regeneration include: (a) the ability to reuse adsorbent; (b) it is cheaper compared to the cost of producing, procuring or synthesizing new adsorbent; and (c) it helps in selenium recovery and post-treatment sludge management to avoid secondary re-contamination of selenium in the environment.

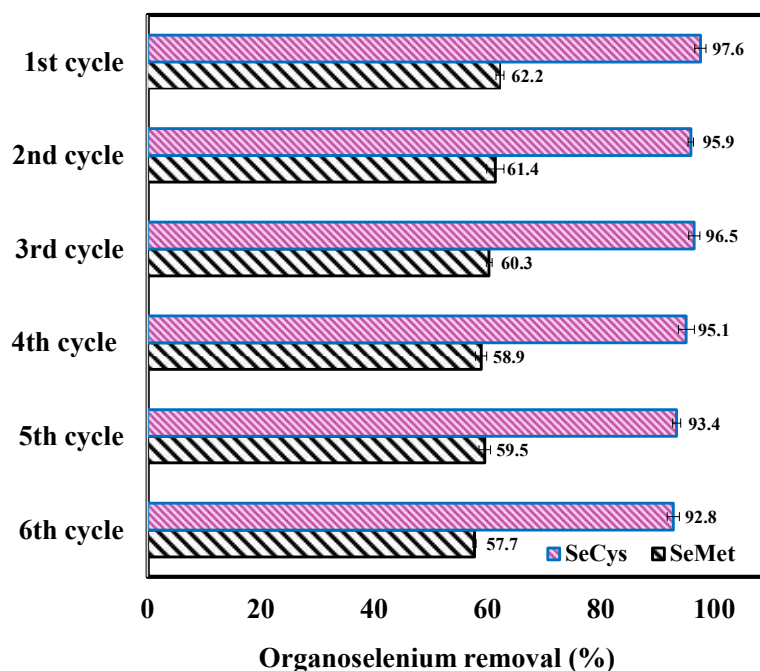


Figure 12. Organoselenium removal using regenerated nZVI/GAC in six treatment cycles. Initial concentration of 0.5 mg/L, 3 g/L, pH 7.0 at 25 °C for 6 h.

4. Mechanism of Removing Organoselenium by nZVI/GAC

The removal mechanism of organoselenium and the changes that occurred during adsorption and post adsorption by nZVI/GAC were analyzed with SEM-EDS as discussed previous sections. Hence, the process of organoselenium adsorption using nZVI/GAC composite is summarized as follows: (i) organoselenium contaminant in the solution was actioned by the adsorption potential on GAC surface and in the pores, (ii) which resulted in the partitioning of organoselenium onto the surface of the adsorbent via adsorption or reduction by the concurrent reaction of the oxide's scale (such as, Fe_3O_4 , $\text{Fe}(\text{OH})_2$ and $\text{Fe}(\text{OH})_3$) that takes place on the adsorbent surface; (iii) overall, organoselenium is adsorbed onto the nZVI/GAC surface.

5. Conclusions

In this study, nZVI/GAC composite was synthesized with the view to explore the advantages of GAC adsorption material and nZVI reductive material to produce a more effective adsorbent to remove organoselenium from wastewater. XRD, BET and SEM imaging results demonstrated that nZVI particles were successfully supported/loaded inside GAC pores. Batch experiments were performed for adsorption of SeMet and SeCys under various conditions—adsorbent dosage studies, pH effects, adsorption kinetics and adsorbate initial concentration studies. NZVI/GAC composite showed a strong affinity to remove organoselenium from wastewater with an optimal dose of 3 g/L. Under various conditions tested, SeCys adsorbed more actively onto nZVI/GAC composite than SeMet, with a maximum removal efficiency of 99.9% and 78.2%, respectively. Change in pH had a remarkable effect on SeCys and SeMet removal by nZVI/GAC; near-neutral and

neutral pH appears to be the most favorable conditions for higher removal efficiency. The results of the initial adsorbate concentration demonstrated that the K_2 decreased with an increase in organoselenium concentration, and in contrast, adsorption capacity (q_e) increased with higher C_0 , irrespective of the adsorbate. The kinetics studies revealed a two-step adsorption process for organoselenium using nZVI/GAC composite. The adsorption process was characterized by PSO model. Langmuir and Freundlich models fitted well with the experimental data. Other than nitrate ions, oxyanions were observed to decrease organoselenium removal efficiency substantially. It was observed that some cations (Ca^{2+} K^+) significantly increased organoselenium removal, under which the maximum removal efficiency was achieved for both SeCys and SeMet. Overall, nZVI/GAC composite can be considered a promising and efficient technology for the removal of organoselenium from wastewater. Advantages of this technology include but are not limited to cost-effectiveness, environmentally friendly, and the swift kinetics in treating organoselenium which can be adapted and utilized in wastewater treatment facilities.

Author Contributions: Conceptualization, S.O.O., G.A. and D.P.; methodology, S.O.O.; experimental design, S.O.O.; validation, S.O.O. and G.A.; formal analysis, S.O.O.; investigation, S.O.O.; resources, G.A.; writing—original draft preparation, S.O.O.; writing—review and editing, G.A. and D.P.; supervision, G.A.; project administration, S.O.O.; funding acquisition, G.A. All authors have read and agreed to the published version of the manuscript.

Funding: Natural Sciences and Engineering Research Council of Canada (NSERC).

Acknowledgments: The authors gratefully acknowledge the funding support provided by Natural Sciences and Engineering Research Council of Canada (NSERC) through an Engage grant and the Petroleum Technology Development Fund (PTDF) Nigeria.

Conflicts of Interest: The authors declare no conflict of interest.

References

1. Kapoor, A.; Tanjore, S.; Viraraghavan, T. Removal of selenium from water and wastewater. *Int. J. Environ. Stud.* **1995**, *49*, 137–147. [[CrossRef](#)]
2. Santos, S.; Ungureanu, G.; Boaventura, R.; Botelho, C. Selenium contaminated waters: An overview of analytical methods, treatment options and recent advances in sorption methods. *Sci. Total Environ.* **2015**, *521*, 246–260. [[CrossRef](#)] [[PubMed](#)]
3. Sun, H.-J.; Rathinasabapathi, B.; Wu, B.; Luo, J.; Pu, L.-P.; Ma, L.Q. Arsenic and selenium toxicity and their interactive effects in humans. *Environ. Int.* **2014**, *69*, 148–158. [[CrossRef](#)] [[PubMed](#)]
4. Dumont, E.; Vanhaecke, F.; Cornelis, R. Selenium speciation from food source to metabolites: A critical review. *Anal. Bioanal. Chem.* **2006**, *385*, 1304–1323. [[CrossRef](#)]
5. Amoako, P.O.; Uden, P.C.; Tyson, J.F. Speciation of selenium dietary supplements; formation of S-(methylseleno) cysteine and other selenium compounds. *Anal. Chim. Acta* **2009**, *652*, 315–323. [[CrossRef](#)]
6. LeBlanc, K.L.; Wallschlagel, D. Production and release of selenomethionine and related organic selenium species by microorganisms in natural and industrial waters. *Environ. Sci. Technol.* **2016**, *50*, 6164–6171. [[CrossRef](#)]
7. Uglietta, R.; Doyle, P.T.; Walker, G.P.; Heard, J.W.; Leddin, C.M.; Stockdale, C.R.; McIntosh, G.H.; Young, G.P.; Dunshea, F.R. Bioavailability of selenium from selenium-enriched milk assessed in the artificially reared neonatal pig. *Nutr. Diet.* **2008**, *65*, S37–S40. [[CrossRef](#)]
8. Maseko, T.; Callahan, D.L.; Dunshea, F.R.; Doronila, A.; Kolev, S.D.; Ng, K. Chemical characterisation and speciation of organic selenium in cultivated selenium-enriched *Agaricus bisporus*. *Food Chem.* **2013**, *141*, 3681–3687. [[CrossRef](#)]
9. Lemly, A.D. Environmental implications of excessive selenium: A review. *Biomed. Environ. Sci.* **1997**, *10*, 415–435.
10. Okonji, S.O.; Yu, L.; Dominic, J.A.; Pernitsky, D.; Achari, G. Adsorption by Granular Activated Carbon and Nano Zerovalent Iron from Wastewater: A Study on Removal of Selenomethionine and Selenocysteine. *Water* **2021**, *13*, 23. [[CrossRef](#)]
11. Manceau, A.; Gallup, D.L. Removal of Selenocyanate in Water by Precipitation: Characterization of Copper–Selenium Precipitate by X-ray Diffraction, Infrared, and X-ray Absorption Spectroscopy. *Environ. Sci. Technol.* **1997**, *31*, 968–976. [[CrossRef](#)]
12. Meng, X.; Bang, S.; Korfiatis, G.P. Removal of selenocyanate from water using elemental iron. *Water Res.* **2002**, *36*, 3867–3873. [[CrossRef](#)]
13. Latva, S.; Peräniemi, S.; Ahlgrén, M. Study of metal-loaded activated charcoals for the separation and determination of selenium species by energy dispersive X-ray fluorescence analysis. *Anal. Chim. Acta* **2003**, *478*, 229–235. [[CrossRef](#)]
14. Okonji, S.O.; Dominic, J.A.; Pernitsky, D.; Achari, G. Removal and recovery of selenium species from wastewater: Adsorption kinetics and co-precipitation mechanisms. *J. Water Process Eng.* **2020**, *38*, 101666. [[CrossRef](#)]

15. Zhu, H.; Jia, Y.; Wu, X.; Wang, H. Removal of arsenic from water by supported nano zero-valent iron on activated carbon. *J. Hazard. Mater.* **2009**, *172*, 1591–1596. [[CrossRef](#)]
16. Xu, P.; Zeng, G.M.; Huang, D.L.; Feng, C.L.; Hu, S.; Zhao, M.H.; Lai, C.; Wei, Z.; Huang, C.; Xie, G.X. Use of iron oxide nanomaterials in wastewater treatment: A review. *Sci. Total Environ.* **2012**, *424*, 1–10. [[CrossRef](#)]
17. Zeng, G.; Liu, Y.; Tang, L.; Yang, G.; Pang, Y.; Zhang, Y.; Zhou, Y.; Li, Z.; Li, M.; Lai, M. Enhancement of Cd (II) adsorption by polyacrylic acid modified magnetic mesoporous carbon. *Chem. Eng. J.* **2015**, *259*, 153–160. [[CrossRef](#)]
18. Wang, W.; Wang, J.; Guo, Y.; Zhu, C.; Pan, F.; Wu, R.; Wang, C. Removal of multiple nitrosamines from aqueous solution by nanoscale zero-valent iron supported on granular activated carbon: Influencing factors and reaction mechanism. *Sci. Total Environ.* **2018**, *639*, 934–943. [[CrossRef](#)]
19. Tang, C.; Huang, Y.H.; Zeng, H.; Zhang, Z. Reductive removal of selenate by zero-valent iron: The roles of aqueous Fe²⁺ and corrosion products, and selenate removal mechanisms. *Water Res.* **2014**, *67*, 166–174. [[CrossRef](#)]
20. Zhang, Y.; Wang, J.; Amrhein, C.; Frankenberger, W.T. Removal of selenate from water by zerovalent iron. *J. Environ. Qual.* **2005**, *34*, 487–495. [[CrossRef](#)]
21. Liang, L.; Jiang, X.; Yang, W.; Huang, Y.; Guan, X.; Li, L. Kinetics of selenite reduction by zero-valent iron. *Desalin. Water Treat.* **2015**, *53*, 2540–2548. [[CrossRef](#)]
22. Choe, S.; Lee, S.-H.; Chang, Y.-Y.; Hwang, K.-Y.; Khim, J. Rapid reductive destruction of hazardous organic compounds by nanoscale Fe⁰. *Chemosphere* **2001**, *42*, 367–372. [[CrossRef](#)]
23. Elliott, D.W.; Lien, H.-L.; Zhang, W.-X. Degradation of lindane by zero-valent iron nanoparticles. *J. Environ. Eng.* **2009**, *135*, 317–324. [[CrossRef](#)]
24. Ambashta, R.D.; Repo, E.; Sillanpää, M. Degradation of tributyl phosphate using nanopowders of iron and iron–nickel under the influence of a static magnetic field. *Ind. Eng. Chem. Res.* **2011**, *50*, 11771–11777. [[CrossRef](#)]
25. Naja, G.; Halasz, A.; Thiboutot, S.; Ampleman, G.; Hawari, J. Degradation of hexahydro-1, 3, 5-trinitro-1, 3, 5-triazine (RDX) using zerovalent iron nanoparticles. *Environ. Sci. Technol.* **2008**, *42*, 4364–4370. [[CrossRef](#)]
26. Klimkova, S.; Cernik, M.; Lacinova, L.; Filip, J.; Jancik, D.; Zboril, R. Zero-valent iron nanoparticles in treatment of acid mine water from in situ uranium leaching. *Chemosphere* **2011**, *82*, 1178–1184. [[CrossRef](#)]
27. Wang, C.-B.; Zhang, W.-x. Synthesizing nanoscale iron particles for rapid and complete dechlorination of TCE and PCBs. *Environ. Sci. Technol.* **1997**, *31*, 2154–2156. [[CrossRef](#)]
28. Zhang, S.; Li, X.; Yang, Y.; Li, Y.; Chen, J.; Ding, F. Adsorption, transformation, and colloid-facilitated transport of nano-zero-valent iron in soils. *Environ. Pollut. Bioavailab.* **2019**, *31*, 208–218. [[CrossRef](#)]
29. Bhattacharjee, S.; Ghoshal, S. Sulfidation of nanoscale zerovalent iron in the presence of two organic macromolecules and its effects on trichloroethene degradation. *Environ. Sci. Nano* **2018**, *5*, 782–791. [[CrossRef](#)]
30. Sarathy, V.; Tratnyek, P.G.; Nurmi, J.T.; Baer, D.R.; Amonette, J.E.; Chun, C.L.; Penn, R.L.; Reardon, E.J. Aging of iron nanoparticles in aqueous solution: Effects on structure and reactivity. *J. Phys. Chem. C* **2008**, *112*, 2286–2293. [[CrossRef](#)]
31. Liu, Y.; Phenrat, T.; Lowry, G.V. Effect of TCE concentration and dissolved groundwater solutes on NZVI-promoted TCE dechlorination and H₂ evolution. *Environ. Sci. Technol.* **2007**, *41*, 7881–7887. [[CrossRef](#)] [[PubMed](#)]
32. Xie, Y.; Cwiertny, D.M. Use of dithionite to extend the reactive lifetime of nanoscale zero-valent iron treatment systems. *Environ. Sci. Technol.* **2010**, *44*, 8649–8655. [[CrossRef](#)] [[PubMed](#)]
33. Eglal, M.M.; Ramamurthy, A.S. Nanofer ZVI: Morphology, particle characteristics, kinetics, and applications. *J. Nanomater.* **2014**, *2014*, 152824. [[CrossRef](#)]
34. Kallel, M.; Belaid, C.; Mechichi, T.; Ksibi, M.; Elleuch, B. Removal of organic load and phenolic compounds from olive mill wastewater by Fenton oxidation with zero-valent iron. *Chem. Eng. J.* **2009**, *150*, 391–395. [[CrossRef](#)]
35. Zhang, N.; Lin, L.-S.; Gang, D. Adsorptive selenite removal from water using iron-coated GAC adsorbents. *Water Res.* **2008**, *42*, 3809–3816. [[CrossRef](#)]
36. Zhang, N.; Gang, D.; Lin, L.-S. Adsorptive removal of parts per million level Selenate using iron-coated GAC Adsorbents. *J. Environ. Eng.* **2010**, *136*, 1089–1095. [[CrossRef](#)]
37. Zelmanov, G.; Semiat, R. Selenium removal from water and its recovery using iron (Fe³⁺) oxide/hydroxide-based nanoparticles sol (NanoFe) as an adsorbent. *Sep. Purif. Technol.* **2013**, *103*, 167–172. [[CrossRef](#)]
38. Langmuir, I. The constitution and fundamental properties of solids and liquids. *Part I. Solids. J. Am. Chem. Soc.* **1916**, *38*, 2221–2295. [[CrossRef](#)]
39. Ling, L.; Pan, B.; Zhang, W.-X. Removal of selenium from water with nanoscale zero-valent iron: Mechanisms of intraparticle reduction of Se (IV). *Water Res.* **2015**, *71*, 274–281. [[CrossRef](#)]
40. Jabeen, H.; Kemp, K.C.; Chandra, V. Synthesis of nano zerovalent iron nanoparticles–graphene composite for the treatment of lead contaminated water. *J. Environ. Manag.* **2013**, *130*, 429–435. [[CrossRef](#)]
41. Li, L.; Fan, M.; Brown, R.C.; Van Leeuwen, J.; Wang, J.; Wang, W.; Song, Y.; Zhang, P. Synthesis, properties, and environmental applications of nanoscale iron-based materials: A review. *Crit. Rev. Environ. Sci. Technol.* **2006**, *36*, 405–431. [[CrossRef](#)]
42. Liu, M.; Wang, Y.; Chen, L.; Zhang, Y.; Lin, Z. Mg(OH)₂ supported nanoscale zero valent iron enhancing the removal of Pb (II) from aqueous solution. *ACS Appl. Mater. Interfaces* **2015**, *7*, 7961–7969. [[CrossRef](#)] [[PubMed](#)]

43. Sheng, G.; Alsaedi, A.; Shammakh, W.; Monaque, S.; Sheng, J.; Wang, X.; Li, H.; Huang, Y. Enhanced sequestration of selenite in water by nanoscale zero valent iron immobilization on carbon nanotubes by a combined batch, XPS and XAFS investigation. *Carbon* **2016**, *99*, 123–130. [[CrossRef](#)]
44. Liu, X.; Lai, D.; Wang, Y. Performance of Pb (II) removal by an activated carbon supported nanoscale zero-valent iron composite at ultralow iron content. *J. Hazard. Mater.* **2019**, *361*, 37–48. [[CrossRef](#)]
45. Liu, Y.; Zeng, Z.; Zeng, G.; Tang, L.; Pang, Y.; Li, Z.; Liu, C.; Lei, X.; Wu, M.; Ren, P. Immobilization of laccase on magnetic bimodal mesoporous carbon and the application in the removal of phenolic compounds. *Bioresour. Technol.* **2012**, *115*, 21–26. [[CrossRef](#)]
46. Sun, Y.-P.; Li, X.-q.; Cao, J.; Zhang, W.-x.; Wang, H.P. Characterization of zero-valent iron nanoparticles. *Adv. Colloid Interface Sci.* **2006**, *120*, 47–56. [[CrossRef](#)]
47. Xiao, J.; Yue, Q.; Gao, B.; Sun, Y.; Kong, J.; Gao, Y.; Li, Q.; Wang, Y. Performance of activated carbon/nanoscale zero-valent iron for removal of trihalomethanes (THMs) at infinitesimal concentration in drinking water. *Chem. Eng. J.* **2014**, *253*, 63–72. [[CrossRef](#)]
48. Noubactep, C. The fundamental mechanism of aqueous contaminant removal by metallic iron. *Water SA* **2010**, *36*, 663–670. [[CrossRef](#)]
49. Reinsch, B.C.; Forsberg, B.; Penn, R.L.; Kim, C.S.; Lowry, G.V. Chemical transformations during aging of zerovalent iron nanoparticles in the presence of common groundwater dissolved constituents. *Environ. Sci. Technol.* **2010**, *44*, 3455–3461. [[CrossRef](#)]
50. Bae, S.; Collins, R.N.; Waite, T.D.; Hanna, K. Advances in surface passivation of nanoscale zerovalent iron: A critical review. *Environ. Sci. Technol.* **2018**, *52*, 12010–12025. [[CrossRef](#)]
51. Yoon, I.-H.; Kim, K.-W.; Bang, S.; Kim, M.G. Reduction and adsorption mechanisms of selenate by zero-valent iron and related iron corrosion. *Appl. Catal. B Environ.* **2011**, *104*, 185–192. [[CrossRef](#)]
52. Lai, B.; Zhou, Y.; Yang, P.; Yang, J.; Wang, J. Degradation of 3, 3'-iminobis-propanenitrile in aqueous solution by Fe₀/GAC micro-electrolysis system. *Chemosphere* **2013**, *90*, 1470–1477. [[CrossRef](#)] [[PubMed](#)]
53. Wu, Y.; Yue, Q.; Ren, Z.; Gao, B. Immobilization of nanoscale zero-valent iron particles (nZVI) with synthesized activated carbon for the adsorption and degradation of Chloramphenicol (CAP). *J. Mol. Liq.* **2018**, *262*, 19–28. [[CrossRef](#)]
54. Thomsen, L.; Wharmby, M.; Riley, D.; Held, G.; Gladys, M. The adsorption and stability of sulfur containing amino acids on Cu [5 3 1]. *Surf. Sci.* **2009**, *603*, 1253–1261. [[CrossRef](#)]
55. Sun, Y.; Li, J.; Huang, T.; Guan, X. The influences of iron characteristics, operating conditions and solution chemistry on contaminants removal by zero-valent iron: A review. *Water Res.* **2016**, *100*, 277–295. [[CrossRef](#)] [[PubMed](#)]
56. Wasewar, K.L.; Prasad, B.; Gulipalli, S. Removal of selenium by adsorption onto granular activated carbon (GAC) and powdered activated carbon (PAC). *CLEAN–Soil Air Water* **2009**, *37*, 872–883. [[CrossRef](#)]
57. Amin, M.N.; Kaneco, S.; Kato, T.; Katsumata, H.; Suzuki, T.; Ohta, K. Removal of thiobencarb in aqueous solution by zero valent iron. *Chemosphere* **2008**, *70*, 511–515. [[CrossRef](#)]
58. Mortazavian, S.; An, H.; Chun, D.; Moon, J. Activated carbon impregnated by zero-valent iron nanoparticles (AC/nZVI) optimized for simultaneous adsorption and reduction of aqueous hexavalent chromium: Material characterizations and kinetic studies. *Chem. Eng. J.* **2018**, *353*, 781–795. [[CrossRef](#)]
59. Mishra, B.; Priyadarsini, K.; Mohan, H. One-Electron Oxidation of Selenomethionine in Aqueous Solutions. *BARC Newsl.* **2005**, *261*, 115.
60. Bettelheim, F.A.; Brown, W.H.; Campbell, M.K.; Farrell, S.O.; Torres, O. *Introduction to General, Organic and Biochemistry*; Nelson Education: Toronto, ON, Canada, 2012.
61. Gosu, V.; Gurjar, B.R.; Surampalli, R.Y.; Zhang, T.C. Treatment of pyridine-bearing wastewater by Nano Zero-valent iron supported on activated carbon derived from agricultural waste. *Desalin. Water Treat.* **2016**, *57*, 6250–6260. [[CrossRef](#)]
62. Zhang, T.C.; Huang, Y.H. Profiling iron corrosion coating on iron grains in a zerovalent iron system under the influence of dissolved oxygen. *Water Res.* **2006**, *40*, 2311–2320. [[CrossRef](#)] [[PubMed](#)]
63. Wu, L.; Liao, L.; Lv, G.; Qin, F.; He, Y.; Wang, X. Micro-electrolysis of Cr (VI) in the nanoscale zero-valent iron loaded activated carbon. *J. Hazard. Mater.* **2013**, *254*, 277–283. [[CrossRef](#)] [[PubMed](#)]
64. Gupta, S.S.; Bhattacharyya, K.G. Kinetics of adsorption of metal ions on inorganic materials: A review. *Adv. Colloid Interface Sci.* **2011**, *162*, 39–58. [[CrossRef](#)] [[PubMed](#)]
65. Allen, S.J.; Gan, Q.; Matthews, R.; Johnson, P.A. Kinetic modeling of the adsorption of basic dyes by kudzu. *J. Colloid Interface Sci.* **2005**, *286*, 101–109. [[CrossRef](#)] [[PubMed](#)]
66. Aksu, Z.; Dönmez, G. A comparative study on the biosorption characteristics of some yeasts for Remazol Blue reactive dye. *Chemosphere* **2003**, *50*, 1075–1083. [[CrossRef](#)]
67. Cermakova, L.; Kopecka, I.; Pivokonsky, M.; Pivokonska, L.; Janda, V. Removal of cyanobacterial amino acids in water treatment by activated carbon adsorption. *Sep. Purif. Technol.* **2017**, *173*, 330–338. [[CrossRef](#)]
68. Tseng, R.-L.; Wu, F.-C. Inferring the favorable adsorption level and the concurrent multi-stage process with the Freundlich constant. *J. Hazard. Mater.* **2008**, *155*, 277–287. [[CrossRef](#)]
69. Davis, J.A.; Leckie, J.O. Surface ionization and complexation at the oxide/water interface. 3. Adsorption of anions. *J. Colloid Interface Sci.* **1980**, *74*, 32–43. [[CrossRef](#)]
70. Goh, K.-H.; Lim, T.-T. Geochemistry of inorganic arsenic and selenium in a tropical soil: Effect of reaction time, pH, and competitive anions on arsenic and selenium adsorption. *Chemosphere* **2004**, *55*, 849–859. [[CrossRef](#)]

71. Bae, S.; Hanna, K. Reactivity of nanoscale zero-valent iron in unbuffered systems: Effect of pH and Fe (II) dissolution. *Environ. Sci. Technol.* **2015**, *49*, 10536–10543. [[CrossRef](#)]
72. Huang, Y.H.; Tang, C.; Zeng, H. Removing molybdate from water using a hybridized zero-valent iron/magnetite/Fe (II) treatment system. *Chem. Eng. J.* **2012**, *200*, 257–263. [[CrossRef](#)]
73. Xu, J.; Hao, Z.; Xie, C.; Lv, X.; Yang, Y.; Xu, X. Promotion effect of Fe_2^+ and Fe_3O_4 on nitrate reduction using zero-valent iron. *Desalination* **2012**, *284*, 9–13. [[CrossRef](#)]